nature physics

PROGRESS ARTICLE

PUBLISHED ONLINE: 31 JULY 2015 | DOI: 10.1038/NPHYS3404

Structured quantum waves

Jérémie Harris[1], Vincenzo Grillo[2], Erfan Mafakheri[3], Gian Carlo Gazzadi[2], Stefano Frabboni[2,3], Robert W. Boyd[1,4] and Ebrahim Karimi[1]*

The study of structured optical waves has enhanced our understanding of light and numerous experimental methods now enable the control of the angular momentum and radial distributions. Recently, these wavestructuring techniques have been successfully applied to the generation and shaping of electron beams, leading to promising practical and fundamental advances. Here, we discuss recent progress in the emerging field of electron beam shaping, and explore the unique attributes that distinguish electron beams from their photonic analogues.

Throughout its orbit around our solar system, a comet's tail invariably points away from the sun. As early as the seventeenth century, this observation led Johannes Kepler to conjecture that sunlight might carry linear momentum. Only in 1905 did John Henry Poynting develop the first theory describing the momentum density of electromagnetic waves[1]. Almost simultaneously, Albert Einstein proposed that light might be comprised of quantized packets of energy. Shortly thereafter, these energy packets, now known as photons[2], were understood to carry quantized momenta $\mathbf{p} = \hbar\mathbf{k}$ as well, where $\hbar$ and $\mathbf{k}$ denote the reduced Planck constant and photon wavevector. Today, optical linear momentum is a well-understood phenomenon that explains countless physical observations, from radiation pressure to Compton scattering. The study of optical linear momentum in media remains active, and this work has recently culminated in a solution to the long-standing Abraham–Minkowski dilemma[3].

Less commonly recognized is the fact that light can carry angular momentum in addition to its linear momentum. This follows from the definition of angular momentum, $\mathbf{j} = \mathbf{r} \times \mathbf{p}$, where $\mathbf{r}$ is the radial vector. The optical angular momentum carried by a paraxial optical beam has two sources[4]: spin angular momentum (SAM), $\mathbf{s}$, and orbital angular momentum (OAM), $\boldsymbol{\ell}$, so that $\mathbf{j} = \mathbf{s} + \boldsymbol{\ell}$. Optical SAM is directly associated with the circular polarization of light, and represents a form of intrinsic angular momentum, as its magnitude is independent of the position about which it is measured. SAM is therefore intimately linked to the vectorial (polarization) structure of a beam[5]. A beam of circularly polarized light necessarily carries SAM, and on interacting with a small particle will cause it to rotate about its centre. The mechanical properties of SAM were first explored by Beth[6], who demonstrated exchanges of angular momentum between circularly polarized light and a doubly refracting plate.

Optical SAM has also drawn interest on fundamental grounds[7]. In particular, an apparent paradox arises in the interaction between circularly polarized optical plane waves and massive particles[8]. Because plane waves are non-localized[9], they represent non-paraxial beams, and therefore their angular momenta cannot be unambiguously separated into SAM and OAM components. Despite their ambiguous SAM content, plane waves do impart a well-defined SAM onto particles with which they interact. This peculiar circumstance can be explained by noting that the only portion of the plane wave that is relevant to the interaction is that which overlaps with the absorbing particle. For the purpose of the interaction, the plane wave can therefore be considered to be a localized and truncated beam, for which the shape and size matches that of the particle, so that it is effectively paraxial, resulting in an unambiguous effective beam SAM (ref. 10).

In contrast to SAM, OAM is associated with a beam's transverse phase profile, rather than its polarization. Optical OAM can be divided into intrinsic OAM, $\boldsymbol{\ell}_{\mathrm{int}}$, and extrinsic OAM, $\boldsymbol{\ell}_{\mathrm{ext}}$ (ref. 11). Whereas intrinsic OAM is constant for a particular beam, extrinsic OAM varies with the axis about which it is measured. When an OAM-carrying beam interacts with a small particle, its extrinsic OAM induces the particle's rotation about the beam axis, whereas its intrinsic OAM causes the particle to rotate about an axis through its centre[12], in a manner resembling the mechanical effect of SAM (refs 13,14). An OAM-carrying beam is described by a 'wavefunction' containing a corkscrew (helical) phase $\exp(i\ell\varphi)$, where ℓ is an integer, and φ is the azimuthal angle in the plane transverse to the beam axis[15]. Such beams therefore have twisted spiral phase fronts (associated with so-called optical vortices), whose cophasal surfaces form ℓ-helices during propagation, and therefore possess non-zero transverse wavevectors. Beams possessing well-defined OAMs are known as 'twisted beams'. Any OAM-carrying beam contains at least one phase singularity, a point of undefined phase in the plane transverse to the beam propagation axis[16].

The scales associated with features of the optical field tied to OAM and SAM are fairly comparable. For SAM, the electric field of a circularly polarized optical beam rotates once after propagating by one wavelength. Similarly, an OAM-carrying beam's cophasal surfaces will experience one full twist after ℓ wavelengths of propagation[17]. Despite their similarities, spin and orbital angular momenta represent independent degrees of freedom for paraxial optical fields in vacuum or isotropic media. Still another independent degree of freedom required to fully characterize the fields' transverse phase and intensity distributions is the mode radial parameter[18]. The radial index p associated with Laguerre–Gauss (LG) modes, which are solutions to the paraxial wave equation, was recently shown to be quantized in the single-photon regime[19], and should not be confused with the beam waist or related parameters.

Indeed the SAM, OAM and radial parameters all represent quantum indices that can be assigned to individual photons. Specifically, single photons can exist in SAM eigenstates, in which

[1]Department of Physics, University of Ottawa, 25 Templeton St., Ottawa, Ontario K1N 6N5, Canada. [2]CNR-Istituto Nanoscienze, Centro S3, Via G Campi 213/a, I-41125 Modena, Italy. [3]Dipartimento di Fisica Informatica e Matematica, Università di Modena e Reggio Emilia, via G Campi 213/a, I-41125 Modena, Italy. [4]Institute of Optics, University of Rochester, Rochester, New York 14627, USA. *e-mail: ekarimi@uottawa.ca

they carry spin angular momenta $s_z = s\hbar$ about their propagation direction; can occupy OAM eigenstates, in which they carry orbital angular momenta $\ell_z = \ell\hbar$ about their propagation direction[20]; and can also exist in radial mode eigenstates, characterized by well-defined radial indices p (for LG (ref. 19), Walsh[21,22] or related modes), where $s = \pm 1$ and $\ell = 0, \pm 1, \pm 2, \ldots$ and $p = 0, 1, 2, \ldots$ are the spin, azimuthal and radial indices. To unambiguously describe the quantum state of a single photon, one therefore must provide information about each of these parameters, in addition to the photon wavevector $\mathbf{k}$. Consequently, a single photon possessing well-defined indices s, ℓ, p and a well-defined wavevector is an excitation of the electromagnetic field, produced by the action of a creation operator $a^{\dagger}_{\mathbf{k};s,p,\ell}$ on a vacuum state state $|0\rangle$, such that $|\mathbf{k}; s, p, \ell\rangle = a^{\dagger}_{\mathbf{k};s,p,\ell}|0\rangle$ (ref. 23). More generally, an arbitrary single-photon nonseparable state may be described by a superposition of s, ℓ, p and $\mathbf{k}$ eigenstates, in which case it may be ascribed a 'wavefunction' $|\Psi\rangle = \sum_{\mathbf{k};s,p,\ell} c^{p,\ell}_{\mathbf{k},s}|\mathbf{k}; s, p, \ell\rangle$, where $c^{p,\ell}_{\mathbf{k},s}$ is a complex constant. Beams whose constituent photons are described by 'wavefunctions' with controlled coefficients $c^{p,\ell}_{\mathbf{k},s}$ are said to be structured. Innumerable examples of such beams exist, including, for example, a category of modes known as radial vector beams, which are characterized by only two non-zero coefficients, $c^{\ell=1}_{s=1} = c^{\ell=-1}_{s=-1} = 1/\sqrt{2}$, whose radial indices p and wavevectors are identical. Radial vector beams possess radially oriented linear polarizations in the plane transverse to their propagation direction, and have found applications in near-field microscopy and lithography[24]. An example of a structured beam is shown in Fig. 1.

Despite their usual independence in vacuum and isotropic media, SAM, OAM and radial indices can be coupled within media in general, and even in vacuum under tight focusing conditions[25]. For example, a Gaussian beam with radial index $p = 0$ and flat phase front $\ell = 0$ can be converted into a superposition of modes with non-zero p values, each carrying one unit of OAM, by passing through a spiral phase plate[26]. Exchanges of angular momentum between the SAM and OAM spaces have also been demonstrated in inhomogeneous birefringent materials, such as photonic[27] and plasmonic[28] q-plates, and liquid crystal droplets[29]. The manipulation of polarization, radial and azimuthal indices has sparked great interest in quantum and classical optics, leading to applications in coronagraphy[30], superdense coding[31] and quantum information[32]. Only recently, however, have optical structuring techniques been applied to the generation and shaping of electron beams.

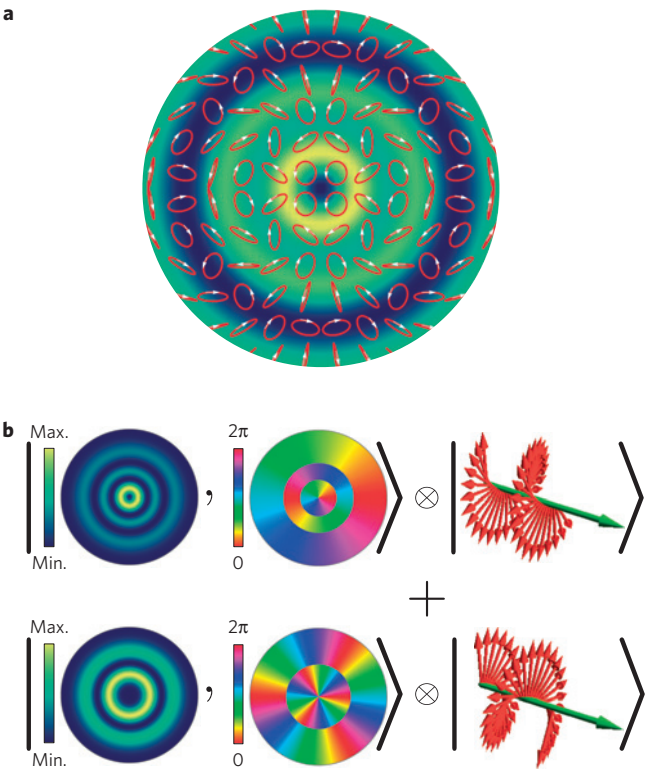

Figure 1 | An example of structured light. a, Composite image showing transverse distributions of polarization and intensity associated with a structured photon beam constructed from an equal superposition of the single-photon states $|\mathbf{k}; s=1, p=2, \ell=1\rangle$ and $|\mathbf{k}; s=-1, p=1, \ell=-3\rangle$, where $|\mathbf{k}; s, p, \ell\rangle$ represents a Laguerre–Gauss (LG) mode propagating along a direction indicated by the wavevector $\mathbf{k}$, with spin, radial and azimuthal parameters respectively denoted s, p and ℓ. Arrows on the polarization ellipses shown in the figure indicate polarization handedness. **b**, Schematic illustrating the transverse intensity, phase and polarization distributions associated with the two component single-photon states that give rise to the pattern shown in **a**. Together, the intensity and phase distributions carry all information conveyed by the ℓ and p transverse indices, and these are therefore combined in the same ket, with the spin index s specified separately.

Electron waves

Since the existence of matter waves was first proposed by de Broglie in 1924, numerous experiments have demonstrated the remarkable correspondence between the wavelike behaviours of matter and light. Electron waves, in particular, have drawn attention in fields from electron microscopy to nanofabrication. The similarities between electron and light waves, now verified theoretically and in countless experiments, suggest that photons' quantum indices can be applied just as well in specifying the states of electrons[33]. However, important distinctions exist between electron and photon waves. Whereas electrons possess a rest mass m_e, a charge e, and obey fermionic statistics, photons are massless, neutral bosons. A related point of contrast is that the non-relativistic (relativistic) wavelike behaviours of electrons and light are prescribed by the Pauli–Schrödinger (Dirac[34]) and Maxwell equations.

Free electrons carry linear momentum given by the de Broglie wave relation as $\hbar k = 2\pi\hbar/\lambda$, where λ is the electron wavelength. Electron wavelengths can be significantly shorter than even those associated with X-rays. This has motivated the development of electron microscopy techniques that exploit short electron wavelengths to achieve sub-ångström resolutions unattainable by standard optical microscopes. More generally in the non-relativistic limit, the linear momentum density of the electron wavefunction $\psi(\mathbf{r}, t)$ is given by $\boldsymbol{\mathcal{P}} = \boldsymbol{\mathcal{P}}_0 + \boldsymbol{\mathcal{P}}_s$, where $\boldsymbol{\mathcal{P}}_0 = \hbar\,\Im(\psi^*\nabla\psi)$, $\boldsymbol{\mathcal{P}}_s = \hbar/4\,\nabla\times(\psi^*\boldsymbol{\sigma}\psi)$, $\boldsymbol{\sigma}$ is the Pauli vector, and $\Im(\cdot)$ denotes the imaginary part of its argument. The momentum density arising from $\boldsymbol{\mathcal{P}}_s$ is always oriented azimuthally, and so makes no net contribution to the linear momentum of the beam. The reason for separating the linear momentum density into $\boldsymbol{\mathcal{P}}_0$ and $\boldsymbol{\mathcal{P}}_s$ components in this way becomes apparent when evaluating the electron angular momentum $\mathbf{J} = \int(\mathbf{r}\times\boldsymbol{\mathcal{P}})\,\mathrm{d}^3\mathbf{r}$. The two momentum density terms $\boldsymbol{\mathcal{P}}_0$ and $\boldsymbol{\mathcal{P}}_s$ respectively produce a coordinate-dependent OAM $\mathcal{L} = \int(\mathbf{r}\times\boldsymbol{\mathcal{P}}_0)\,\mathrm{d}^3\mathbf{r}$ and a coordinate-independent spin angular momentum, $\mathbf{S} = \int(\mathbf{r}\times\boldsymbol{\mathcal{P}}_s)\,\mathrm{d}^3\mathbf{r}$. This spin is quantized: $\mathbf{S} = \hbar\boldsymbol{\sigma}/2$ (ref. 35). From this discussion, it can be seen that electron spin is inextricably linked to the linear momentum distribution in the transverse plane, and hence can act as an important structural parameter for electron wavefunctions[7]. Major electron structural features tied to spin and orbital angular momentum are illustrated in Fig. 2.

It may be slightly surprising to find that the electron spin and photon SAM spaces have the same dimensionality, given that the electron is a fermion, and the photon a boson. This can

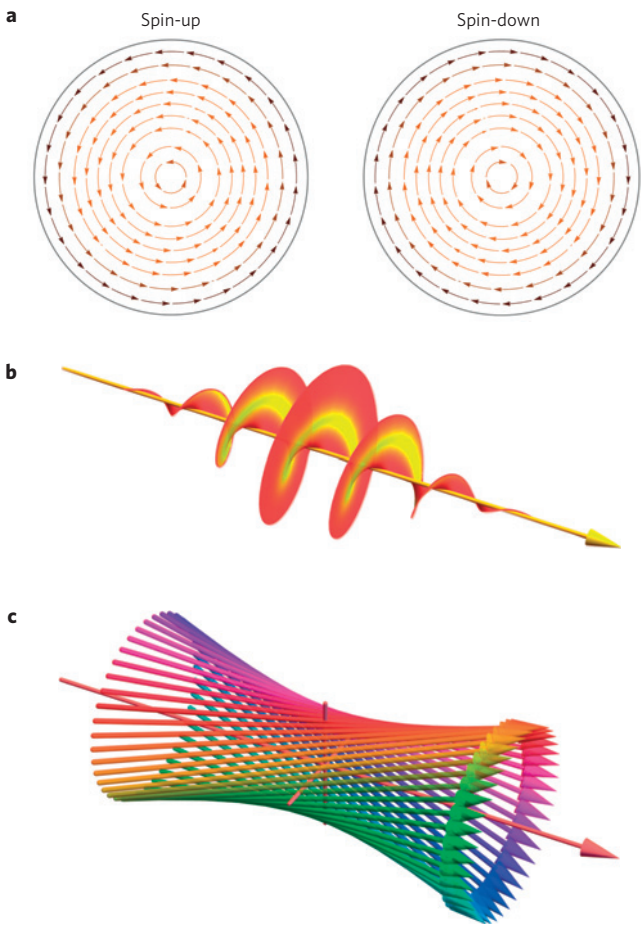

Figure 2 | Electron structural features associated with angular momentum. a, Schematic displaying the spin-dependent transverse linear momentum distributions respectively associated with spin-up ($s=1/2$) and spin-down ($s=-1/2$) electron beams. The electron spin gives rise to a vanishing net transverse linear momentum. **b**, Cophasal surfaces associated with an electron wavepacket carrying OAM $\ell=1$. Intensity is indicated by colour, with yellow (red) denoting the regions of highest (lowest) transverse probability. **c**, Classical (Bohmian) trajectories of individual electrons propagating in a Laguerre–Gauss mode characterized by an azimuthal index $\ell=1$. Colours are used to indicate the phases associated with each electron trajectory.

be explained with an appeal to special relativity, which suggests that a photon's longitudinal polarization must experience infinite length contraction, because the photon travels at the speed of light. Therefore, despite being a spin-1 particle, the photon can effectively access only two (transverse) degrees of freedom, producing the observed correspondence between light and electron waves, in this regard.

When bound to atomic nuclei, electrons possess OAM in addition to their spin. Perhaps more surprisingly, however, even free electrons can be made to carry OAM on propagation[33]. This occurs owing to the presence of transverse components of the electron linear momentum $\boldsymbol{\mathcal{P}}_0$. As with OAM-carrying photon beams, such electron wavefunctions possess spiral phase structures, their wavefunctions containing phase terms $\exp(i\ell\varphi)$. The similarities between the descriptions of electron wavefunctions and photon beams arise from the spinless free particle Schrödinger equation (SFSE), $i\hbar\,\partial_t\psi(\mathbf{r};t)=-\hbar^2/(2m_e)\,\nabla^2\psi(\mathbf{r};t)$. When the SFSE is solved with the ansatz $\psi(\mathbf{r};t)=\psi(\mathbf{r})\,\exp(-iEt/\hbar)$, one obtains the expression $(\nabla^2+k_e^2)\psi(\mathbf{r})=0$, where $k_e^2:=2m_eE/\hbar^2$. This formula is formally identical to the optical wave equation, so that the transverse electron wavefunctions obtained from it will match the transverse modes of the electric field associated with photon beams. When solved in cylindrical coordinates r,φ,z, this form of the SFSE gives rise to a family of Bessel beam solutions, for which the time-independent wavefunctions are given by $\psi(\mathbf{r})\propto J_\ell(k_\perp r)\exp(i(k_\parallel z+\ell\varphi))$ (ref. 36), where J_ℓ is an ℓth order Bessel function of the first kind, and which have well-studied photonic analogues[37]. Bessel modes are diffractionless, non-normalizable, and therefore unphysical solutions to the SFSE and the optical wave equation. If it is assumed that the mode longitudinal wavenumber, $k_\parallel$, is much larger than the transverse wavenumber, $k_\perp=\sqrt{k_e^2-k_\parallel^2}$, the SFSE reduces to a form analogous to the optical paraxial wave equation. The resulting expression possesses solutions in the form of LG modes, introduced earlier for photon beams. Such modes have transverse wavefunctions $|p,\ell\rangle$ at any given axial position z, which in the position representation are expressed as $\psi^{\mathrm{LG}}_{p,\ell}(r,\varphi;z):=\langle r,\varphi,z|p,\ell\rangle$, and have been extensively studied[38].

Electron wavefunctions possessing phase terms $\exp(i\ell\varphi)$ and $\exp(ik_\parallel z)$, such as Bessel and LG modes, carry OAM $\hbar\ell$ and linear momenta $\hbar k_\parallel$ per electron, oriented along their propagation direction. Such wavefunctions have linear momentum densities $\boldsymbol{\mathcal{P}}_\ell(r)=\hbar(\ell/r\,\boldsymbol{\varphi}+k_\parallel\,\mathbf{z})\rho_\ell(r)$, and probability current densities $\mathbf{j}_\ell(r)=\boldsymbol{\mathcal{P}}_\ell/m_e$, where $\boldsymbol{\varphi}$ and $\mathbf{z}$ denote the azimuthal and axial unit vectors, and $\rho_\ell(r):=|\psi(r)|^2$. Because electrons carry charge, the presence of an azimuthal probability current produces an effective loop of charge current about the propagation axis[39]. This supplements the charge current already present due to the intrinsic SAM of the electron wavefunction. These spin and OAM-induced charge currents respectively produce magnetic moments $sg_e\mu_B$ and $\ell\mu_B$, where $\mu_B=e\hbar/(2m_e)$ is the electron Bohr magneton, $s=\pm1/2$ is the electron spin index and $g_e\simeq2.002$ is the electron g-factor[34]. These magnetic moments allow interactions between the electron wavefunction and external magnetic fields, which cannot occur for analogous photon beams. Just as remarkably, the OAM carried by twisted electron beams has even been shown to give rise to electric and magnetic fields associated with these beams themselves, which differ significantly from the fields associated with electron beams carrying no OAM (ref. 40).

As with photon beams, an additional radial parameter is required to fully specify the transverse field distributions of electron wavefunctions. This parameter can be discrete or continuous, depending on the electron mode. Bessel modes possess continuous radial parameters $k_\perp$, whereas LG modes possess discretized radial indices p. In either case, the radial parameter dictates the quantization condition for the transverse component of the electron wavefunction's energy; as $k_\perp$ or p increase, so does the transverse energy carried by the electron wavefunction[41,42]. The radial index-dependence of the electron transverse energy is an important consideration in electron/magnetic field interactions[43] and plays a crucial role in electron/electron interactions as well.

Together, the radial, azimuthal and spin indices confer spatial structure on an electron wavefunction, and, along with linear momentum, unambiguously specify the states of individual electrons. Recently, great progress has been made in efforts to produce electron beams with tailored structure, by controlling these parameters.

Experimental generation of structured electron waves

Structured electron beam generation was first reported by Uchida and Tonomura in 2010 (ref. 44), using spiral phase plates consisting of spontaneously stacked graphite thin films to impart OAM onto incident electron beams. Spiral phase plates are produced by inducing azimuthally and uniformly increasing 'optical' thicknesses $t(r,\varphi)$ around the axis of 'optically' dense materials[45]. If the optical thickness of a material can be increased by ℓ de Broglie wavelengths over one full rotation about the phase plate's axis, $\oint\nabla t(r,\varphi)\cdot\mathrm{d}\boldsymbol{\varphi}=\lambda\ell$, the plate will imprint a helical phase

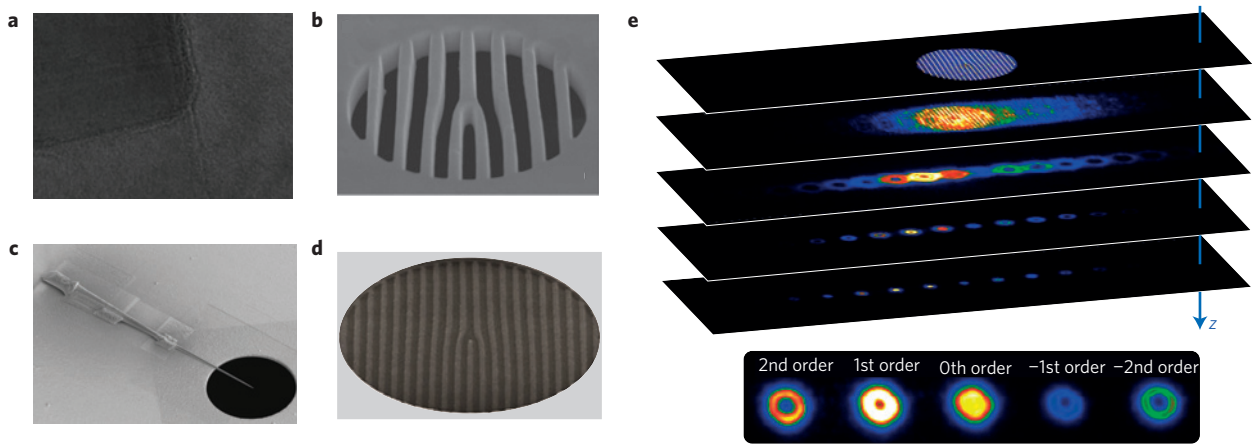

Figure 3 | Electron structuring techniques. a, Scanning electron microscope (SEM) image of a spontaneously stacked graphite sheet (on the nanometre scale), used as a spiral phase plate[44] to impart OAM on an incident electron beam. **b**, SEM image of an amplitude hologram (on the micrometre scale) applied to the generation of twisted electron beams[46]. **c**, SEM image of an ultrathin needle[55] (on the micrometre scale) to simulate a magnetic monopole, capable of imparting OAM on incident electron plane waves. **d**, SEM image of the first electron phase hologram[49] (on the micrometre scale). **e**, Schematic of the structured electron beams emerging from an electron phase hologram. The spreading of various diffraction orders can be observed to occur rapidly on propagation, and the distinct transverse profiles associated with five different diffracted orders are shown in the bottom inset.

$\exp(i\ell\varphi)$ on any incident electron wavefunction. Although the stacked graphite films used to structure the azimuthal phases of electron wavefunctions were found to produce structured beams of reasonable quality, the approach taken in this work could not readily be generalized to produce beams with $|\ell| \neq 1$, as it depended on the isolation of spontaneously stacked graphite films, which could not be produced at will or in customized configurations by an experimenter.

A second seminal study was carried out shortly thereafter, demonstrating the conferral of OAM to electron beams by using amplitude holograms constructed from 100-nm-thick platinum foil[46]. This investigation followed earlier work, which in 2009 also proposed the use of such holograms for structured electron beam generation[47]. This technique benefits from greater versatility, and allows for the generation of electron beams with high OAM content. Amplitude holograms are constructed by simulating the intensity pattern $I_{\mathrm{int}}(r,\varphi)$ produced from the interference of reference $\psi_{\mathrm{ref}}(r,\varphi)$ and desired target $\psi_{\mathrm{t}}(r,\varphi)$ wavefunctions, such that $I_{\mathrm{int}}(r,\varphi) = |\psi_{\mathrm{ref}}(r,\varphi) + \psi_{\mathrm{t}}(r,\varphi)|^2$, and by designing a mask with thickness function $t(r,\varphi) = t_0\,\Theta[I_{\mathrm{int}}(r,\varphi)]$, where $\Theta[\cdot]$ denotes the Heaviside function, and t_0 is the optical thickness of the mask[48]. When an electron beam is made incident on such a hologram, a series of diffracted beams are produced, each carrying a different OAM.

For three years, the holographic generation of structured electron beams was only possible using amplitude holograms. In 2014, however, a new class of holographic mask, already widely used in photon optics and known as the phase hologram, was reported to achieve electron beam shaping by directly imprinting controllable phases onto electron wavefunctions, resulting in unprecedented high efficiencies and low absorption losses[49,50]. This technique was shown to produce high-quality electron Bessel[36] and LG beams, with various azimuthal parameters ℓ.

Following this early work, a number of studies explored applications of holographic masks to the generation of electron beams with high OAM, some achieving values up to $200\hbar$ per electron[51,52]. In a striking demonstration of the effectiveness of phase holograms, one study reported the successful generation of electron Airy beams[53], and observed their unusual transverse 'acceleration' and 'self-healing' properties.

In addition to the spiral phase plate and holographic techniques, a number of alternative approaches also allow for electron beam shaping. One study reported the generation of electron beams with helical phase fronts by manipulating aberrations associated with the corrector lenses of an electron microscope[54], achieving generation efficiencies of 32%. Another demonstrated twisting of electron beams using a simulated magnetic monopole constructed from a thin, nanoscale magnetic needle[55]. This latter strategy could benefit from an unusually high conversion efficiency. An additional advantage distinguishing this magnetic needle method from other electron beam shaping techniques is its independence from the acceleration voltage applied to incident electrons. A variety of distinct strategies therefore exist to generate electrons with structured azimuthal phases. In contrast, little work has been done, as yet, on structuring the radial parameters of electron beams. Electron spin has also received relatively little attention in this regard, despite also being an important structural parameter. This is largely due to the challenge of generating spin-polarized free electron (SPFE) beams; indeed, the generation of SPFEs was thought to be disallowed by Pauli, whose view was later echoed by Bohr in his statement that[56], 'it is impossible to observe the spin of the electron, separated fully from its orbital momentum, by means of experiments based on the concept of classical particle trajectories.' Recently, however, a strategy has been proposed to produce SPFEs by passing an unpolarized electron beam through a magnetic phase grating[57]. Another approach has been proposed to address this challenge, employing complementary and topologically charged electric and magnetic fields to couple electron spin and orbital angular momentum degrees of freedom, producing a spin-polarized, OAM-carrying electron beam[58]. When this beam is phase flattened, a spin-polarized Gaussian electron wavefunction is recovered, with theoretical efficiencies and degrees of polarization of up to 50% and 97.5%, respectively. Various electron structuring strategies are illustrated in Fig. 3.

Outlook

Much theoretical work has been done with a view to applying the unique properties of electron beams to various measurement schemes, and to the study of fundamental physics. For example, a thorough treatment of the interaction between electron beams and magnetic fields was reported in 2012 (ref. 39), showing how the radial intensity and charge current distributions of LG and Bessel electron beams are altered by their propagation through regions containing different magnetic field

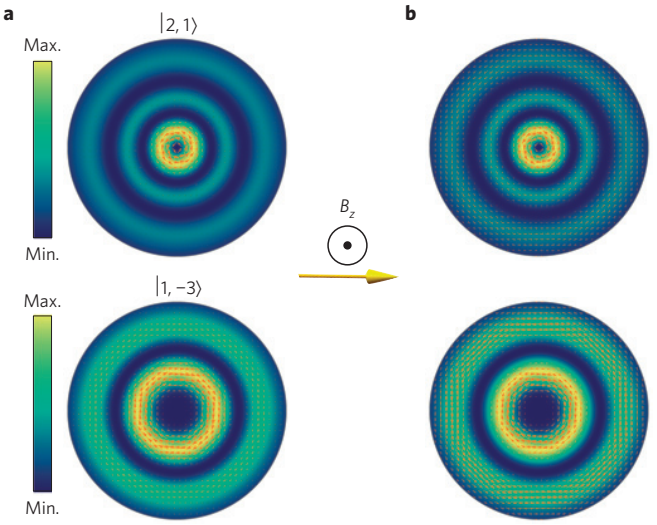

Figure 4 | Structured electron beams and their interaction with uniform magnetic fields. a, Transverse intensity and charge current distributions associated with electron states $|p=2,\ell=1\rangle$ and $|p=1,\ell=-3\rangle$ in the absence of any external magnetic fields, where $|p,\ell\rangle$ denotes an LG mode with radial and azimuthal parameters p and ℓ. The size and orientation of the arrows show the respective magnitude and direction of the local charge current density; the probability density is indicated by colour. **b**, Intensity and charge current distributions associated with the electron wavefunctions shown in **a**, in the presence of a uniform external magnetic field. The beams shown in **a** and **b** are plotted so as to possess identical beam waists for ease of comparison.

configurations. It was found that electron Bessel beams take the form $\psi_{\text{Bessel}} \propto J_{|\ell-\alpha|}(k_\perp r)\exp i(\ell\varphi - k_\parallel z)$ when propagating along a line of magnetic flux proportional to the flux parameter α, so that changes in its magnitude lead to changes in the order of the beam's transverse mode. The effect of external magnetic fields on specific Laguerre–Gauss modes are illustrated in Fig. 4. Additional theoretical studies have since explored the possibility of imparting OAM onto electron beams by means of photon–electron interactions[59]. Electric and magnetic field effects provide a promising avenue for the shaping of electron beams. Electron beams' magnetic field sensitivity might also be exploited for magnetic field sensing in materials science[60]. Further still, recent work has proposed the potential application of structured electron beams to the selective excitation of atomic states, via a transfer of intrinsic electron OAM to electrons in individual atoms[61,62]. As this intrinsic OAM transfer is likely to be significantly less efficient in the case of photon/atom interactions, structured electron beams therefore represent a possible avenue for the exploration of truly novel physical effects.

Structured electron beams have also been considered as tools in the study of polarization radiation (PR) and related phenomena. PR arises from the movement of electrons within spatially inhomogeneous media, which induces a polarization current density in the materials. The magnitude of the PR produced by an electron is proportional to its angular momentum. Observation of PR has proven elusive, however, owing to the small magnitude of the electron intrinsic spin. This limitation could be overcome by using structured electron waves with high OAM values[63].

Further, a recent theoretical study exploring the exotic features of certain structured fermion beams in the relativistic regime demonstrated that such beams could behave as if under the influence of 'virtual forces', even in the total absence of external potentials[64]. This suggests that structured electron beams could in principle be used to simulate the effects of potentials and forces on electrons and other fermions. Remarkably, this study also revealed that certain tailored structures imparted on fermion beams can cause these beams' constituent particles to experience controllable time dilation and length contraction effects. This observation indicates a host of experimental possibilities, including applications in which decaying particles might have their lifetimes extended to a controllable degree using these relativistic effects.

Advances in beam structuring have already paved the way to major developments in many areas. As a new and rapidly advancing field, electron beam shaping holds a wealth of potential for the study of hitherto inaccessible physical phenomena, and the development of novel and exciting applications in electron microscopy and related areas[65,66].

Received 8 April 2015; accepted 15 June 2015;
published online 31 July 2015

References

1. Loudon, R. & Baxter, C. Contributions of John Henry Poynting to the understanding of radiation pressure. *Proc. R. Soc. A* **468,** 1825–1838 (2012).
2. Einstein, A. Über einen die erzeugung und verwandlung des lichtes betreffenden heuristischen gesichtspunkt. *Ann. Phys.* **322,** 132–148 (1905).
3. Barnett, S. M. Resolution of the Abraham–Minkowski dilemma. *Phys. Rev. Lett.* **104,** 070401 (2010).
4. Darwin, C. Notes on the theory of radiation. *Proc. R. Soc. Lond. A* **136,** 36–52 (1932).
5. Poynting, J. The wave motion of a revolving shaft, and a suggestion as to the angular momentum in a beam of circularly polarised light. *Proc. R. Soc. Lond. A* **82,** 560–567 (1909).
6. Beth, R. A. Mechanical detection and measurement of the angular momentum of light. *Phys. Rev.* **50,** 115–125 (1936).
7. Ohanian, H. C. What is spin? *Am. J. Phys.* **54,** 500–505 (1986).
8. Khrapko, R. Question# 79. does plane wave not carry a spin? *Am. J. Phys.* **69,** 405–405 (2001).
9. Humblet, J. Sur le moment d'impulsion d'une onde electromagnetique. *Physica* **10,** 585–603 (1943).
10. Allen, L. & Padgett, M. Response to question# 79. does a plane wave carry spin angular momentum? *Am. J. Phys.* **70,** 567–568 (2002).
11. O'Neil, A., MacVicar, I., Allen, L. & Padgett, M. Intrinsic and extrinsic nature of the orbital angular momentum of a light beam. *Phys. Rev. Lett.* **88,** 053601 (2002).
12. He, H., Friese, M., Heckenberg, N. & Rubinsztein-Dunlop, H. Direct observation of transfer of angular momentum to absorptive particles from a laser beam with a phase singularity. *Phys. Rev. Lett.* **75,** 826–829 (1995).
13. Simpson, N., Dholakia, K., Allen, L. & Padgett, M. Mechanical equivalence of spin and orbital angular momentum of light: An optical spanner. *Opt. Lett.* **22,** 52–54 (1997).
14. Padgett, M. & Bowman, R. Tweezers with a twist. *Nature Photon.* **5,** 343–348 (2011).
15. Allen, L., Beijersbergen, M. W., Spreeuw, R. & Woerdman, J. Orbital angular momentum of light and the transformation of Laguerre–Gaussian laser modes. *Phys. Rev. A* **45,** 8185–8189 (1992).
16. Berry, M. V. Paraxial beams of spinning light. *Proc. SPIE* **3487,** http://dx.doi.org/cbmvrn (1998).
17. Paterson, L. *et al.* Controlled rotation of optically trapped microscopic particles. *Science* **292,** 912–914 (2001).
18. Karimi, E. & Santamato, E. Radial coherent and intelligent states of paraxial wave equation. *Opt. Lett.* **37,** 2484–2486 (2012).
19. Karimi, E. *et al.* Exploring the quantum nature of the radial degree of freedom of a photon via Hong-Ou-Mandel interference. *Phys. Rev. A* **89,** 013829 (2014).
20. Mair, A., Vaziri, A., Weihs, G. & Zeilinger, A. Entanglement of the orbital angular momentum states of photons. *Nature* **412,** 313–316 (2001).
21. Walsh, J. L. A closed set of normal orthogonal functions. *Am. J. Math.* **45,** 5–24 (1923).
22. Salakhutdinov, V., Eliel, E. & Löffler, W. Full-field quantum correlations of spatially entangled photons. *Phys. Rev. Lett.* **108,** 173604 (2012).
23. Romero, L. D., Andrews, D. & Babiker, M. A quantum electrodynamics framework for the nonlinear optics of twisted beams. *J. Opt. B* **4,** S66–S72 (2002).
24. Dorn, R., Quabis, S. & Leuchs, G. Sharper focus for a radially polarized light beam. *Phys. Rev. Lett.* **91,** 233901 (2003).
25. Zhao, Y., Edgar, J. S., Jeffries, G. D., McGloin, D. & Chiu, D. T. Spin-to-orbital angular momentum conversion in a strongly focused optical beam. *Phys. Rev. Lett.* **99,** 073901 (2007).

26. Karimi, E., Zito, G., Piccirillo, B., Marrucci, L. & Santamato, E. Hypergeometric-Gaussian modes. *Opt. Lett.* **32,** 3053–3055 (2007).
27. Marrucci, L., Manzo, C. & Paparo, D. Optical spin-to-orbital angular momentum conversion in inhomogeneous anisotropic media. *Phys. Rev. Lett.* **96,** 163905 (2006).
28. Karimi, E. *et al.* Generating optical orbital angular momentum at visible wavelengths using a plasmonic metasurface. *Light* **3,** e167 (2014).
29. Brasselet, E., Murazawa, N., Misawa, H. & Juodkazis, S. Optical vortices from liquid crystal droplets. *Phys. Rev. Lett.* **103,** 103903 (2009).
30. Foo, G. *et al.* Optical vortex coronagraph. *Opt. Lett.* **30,** 3308–3310 (2005).
31. Barreiro, J. T., Wei, T.-C. & Kwiat, P. G. Beating the channel capacity limit for linear photonic superdense coding. *Nature Phys.* **4,** 282–286 (2008).
32. Molina-Terriza, G., Torres, J. P. & Torner, L. Twisted photons. *Nature Phys.* **3,** 305–310 (2007).
33. Bliokh, K. Y., Bliokh, Y. P., Savel'ev, S. & Nori, F. Semiclassical dynamics of electron wave packet states with phase vortices. *Phys. Rev. Lett.* **99,** 190404 (2007).
34. Bliokh, K. Y., Dennis, M. R. & Nori, F. Relativistic electron vortex beams: Angular momentum and spin–orbit interaction. *Phys. Rev. Lett.* **107,** 174802 (2011).
35. Pauli, W. Über den Zusammenhang des Abschlusses der Elektronengruppen im Atom mit der Komplexstruktur der Spektren. *Z. Phys. A* **31,** 765–783 (1925).
36. Grillo, V. *et al.* Generation of nondiffracting electron Bessel beams. *Phys. Rev. X* **4,** 011013 (2014).
37. Durnin, J. Exact solutions for nondiffracting beams. i. The scalar theory. *J. Opt. Soc. Am.* **4,** 651–654 (1987).
38. Siegman, A. E. *Lasers* (Mill Valley, 1986).
39. Bliokh, K. Y., Schattschneider, P., Verbeeck, J. & Nori, F. Electron vortex beams in a magnetic field: A new twist on Landau levels and Aharonov–Bohm states. *Phys. Rev. X* **2,** 041011 (2012).
40. Lloyd, S. M., Babiker, M., Yuan, J. & Kerr-Edwards, C. Electromagnetic vortex fields, spin, and spin–orbit interactions in electron vortices. *Phys. Rev. Lett.* **109,** 254801 (2012).
41. Greenshields, C., Stamps, R. L. & Franke-Arnold, S. Vacuum Faraday effect for electrons. *New J. Phys.* **14,** 103040 (2012).
42. Guzzinati, G., Schattschneider, P., Bliokh, K. Y., Nori, F. & Verbeeck, J. Observation of the Larmor and Gouy rotations with electron vortex beams. *Phys. Rev. Lett.* **110,** 093601 (2013).
43. Schattschneider, P. *et al.* Imaging the dynamics of free-electron Landau states. *Nature Commun.* **5,** 4586 (2014).
44. Uchida, M. & Tonomura, A. Generation of electron beams carrying orbital angular momentum. *Nature* **464,** 737–739 (2010).
45. Beijersbergen, M., Coerwinkel, R., Kristensen, M. & Woerdman, J. Helical-wavefront laser beams produced with a spiral phaseplate. *Opt. Commun.* **112,** 321–327 (1994).
46. Verbeeck, J., Tian, H. & Schattschneider, P. Production and application of electron vortex beams. *Nature* **467,** 301–304 (2010).
47. McMoran, B. *Electron Diffraction and Interferometry Using Nanostructure* PhD thesis, Univ. Arizona (2009).
48. Bazhenov, V. Y., Vasnetsov, M. & Soskin, M. Laser beams with screw dislocations in their wavefronts. *JETP Lett.* **52,** 429–431 (1990).
49. Grillo, V. *et al.* Highly efficient electron vortex beams generated by nanofabricated phase holograms. *Appl. Phys. Lett.* **104,** 043109 (2014).
50. Shiloh, R., Lereah, Y., Lilach, Y. & Arie, A. Sculpturing the electron wave function using nanoscale phase masks. *Ultramicroscopy* **144,** 26–31 (2014).
51. McMorran, B. J. *et al.* Electron vortex beams with high quanta of orbital angular momentum. *Science* **331,** 192–195 (2011).
52. Grillo, V. *et al.* Holographic generation of highly twisted electron beams. *Phys. Rev. Lett.* **114,** 034801 (2015).
53. Voloch-Bloch, N., Lereah, Y., Lilach, Y., Gover, A. & Arie, A. Generation of electron Airy beams. *Nature* **494,** 331–335 (2013).
54. Clark, L. *et al.* Exploiting lens aberrations to create electron-vortex beams. *Phys. Rev. Lett.* **111,** 064801 (2013).
55. Béché, A., Van Boxem, R., Van Tendeloo, G. & Verbeeck, J. Magnetic monopole field exposed by electrons. *Nature Phys.* **10,** 26–29 (2014).
56. Garraway, B. & Stenholm, S. Does a flying electron spin? *Contemp. Phys.* **43,** 147–160 (2002).
57. McGregor, S., Bach, R. & Batelaan, H. Transverse quantum Stern-Gerlach magnets for electrons. *New J. Phys.* **13,** 065018 (2011).
58. Karimi, E., Marrucci, L., Grillo, V. & Santamato, E. Spin-to-orbital angular momentum conversion and spin-polarization filtering in electron beams. *Phys. Rev. Lett.* **108,** 044801 (2012).
59. Hayrapetyan, A. G. *et al.* Interaction of relativistic electron-vortex beams with few-cycle laser pulses. *Phys. Rev. Lett.* **112,** 134801 (2014).
60. Lloyd, S., Babiker, M. & Yuan, J. Quantized orbital angular momentum transfer and magnetic dichroism in the interaction of electron vortices with matter. *Phys. Rev. Lett.* **108,** 074802 (2012).
61. Yuan, J., Lloyd, S. M. & Babiker, M. Chiral-specific electron-vortex-beam spectroscopy. *Phys. Rev. A* **88,** 031801(R) (2013).
62. Schattschneider, P., Löffler, S., Stöger-Pollach, M. & Verbeeck, J. Is magnetic chiral dichroism feasible with electron vortices? *Ultramicroscopy* **136,** 81–85 (2014).
63. Ivanov, I. P. & Karlovets, D. V. Polarization radiation of vortex electrons with large orbital angular momentum. *Phys. Rev. A* **88,** 043840 (2013).
64. Kaminer, I., Nemirovsky, J., Rechtsman, M., Bekenstein, R. & Segev, M. Self-accelerating Dirac particles and prolonging the lifetime of relativistic fermions. *Nature Phys.* **11,** 261–267 (2015).
65. Verbeeck, J. *et al.* Atomic scale electron vortices for nanoresearch. *Appl. Phys. Lett.* **99,** 203109 (2011).
66. Lloyd, S., Babiker, M. & Yuan, J. Mechanical properties of electron vortices. *Phys. Rev. A* **88,** 031802 (2013).

Acknowledgements

J.H., R.W.B. and E.K. acknowledge the support of the Canada Excellence Research Chairs (CERC) Program.

Additional information

Reprints and permissions information is available online at www.nature.com/reprints. Correspondence should be addressed to E.K.

Competing financial interests

The authors declare no competing financial interests.